JOURNAL OF VIROLOGY, Oct. 2000, p. 9184–9196 Vol. 74, No. 19
0022-538X/00/$04.00+0

Endocytosis and Nuclear Trafficking of Adeno-Associated Virus Type 2 Are Controlled by Rac1 and Phosphatidylinositol-3 Kinase Activation

SALIH SANLIOGLU,[1,2] PETER K. BENSON,[1,3] JUSAN YANG,[1] E. MORREY ATKINSON,[4] THOMAS REYNOLDS,[4] AND JOHN F. ENGELHARDT[1,2]*

Department of Anatomy and Cell Biology and Center for Gene Therapy,[1] Department of Internal Medicine,[2] and Department of Otolaryngology-Head and Neck Surgery Institute,[3] University of Iowa College of Medicine, Iowa City, Iowa 52242, and Targeted Genetics Corporation, Seattle, Washington 98101[4]

Received 12 May 2000/Accepted 14 July 2000

Adeno-associated virus (AAV) is a single-stranded DNA parvovirus that causes no currently known pathology in humans. Despite the fact that this virus is of increasing interest to molecular medicine as a vector for gene delivery, relatively little is known about the cellular mechanisms controlling infection. In this study, we have examined endocytic and intracellular trafficking of AAV-2 using fluorescent (Cy3)-conjugated viral particles and molecular techniques. Our results demonstrate that internalization of heparan sulfate proteoglycan-bound AAV-2 requires αVβ5 integrin and activation of the small GTP-binding protein Rac1. Following endocytosis, activation of a phosphatidylinositol-3 (PI3) kinase pathway was necessary to initiate intracellular movement of AAV-2 to the nucleus via both microfilaments and microtubules. Inhibition of Rac1 using a dominant N17Rac1 mutant led to a decrease in AAV-2-mediated PI3 kinase activation, indicating that Rac1 may act proximal to PI3 kinase during AAV-2 infection. In summary, our results indicate that αVβ5 integrin-mediated endocytosis of AAV-2 occurs through a Rac1 and PI3 kinase activation cascade, which directs viral movement along the cytoskeletal network to the nucleus.

Adeno-associated virus (AAV) is a nonpathogenic, single-stranded DNA human parvovirus that is under development as a gene therapy vector (1, 22, 29, 63). Recombinant AAV-2 (rAAV) carrying reporter genes has been shown to readily transduce several organs, including muscle, brain, and eye (2, 7, 21, 29, 63). However, the transduction efficiency of rAAV appears to vary greatly among different tissues. In part, the lack of AAV-2 cell surface receptors (56) is thought to contribute to the inefficient infection of different tissue types (16).

The nuclear events influencing rAAV transduction, such as the phosphorylation status of the D-sequence-binding protein and the conversion of single-stranded DNA genomes to circular forms, have been partially elucidated (14, 15, 48, 51–53). However, the mechanisms underlying rAAV uptake and trafficking to the nucleus still remain largely undefined. The identification of several receptors and coreceptors has contributed to the understanding of AAV-2 binding to cells, the first step required for internalization. Heparan sulfate proteoglycan (HSPG), the first identified receptor for AAV-2 (56), appears to function primarily in virus attachment to the cell surface. Efficient AAV-2 infection has also been suggested to require a second coreceptor, such as human fibroblast growth factor receptor 1 (47) or αVβ5 integrins (55). Integrins are molecules involved in cell adhesion and motility (9, 33) and have also been implicated in adenovirus infection. In this context, integrins interact with small intracellular signaling molecules, such as Rho, Rac, and Cdc42 GTPases, and can act through actin fibers to facilitate motility and endocytic pathways (42, 45). Furthermore, integrin clustering has been shown to activate a focal adhesion kinase, known as $pp125^{FAK}$, through tyrosine phosphorylation (39). Tyrosine-phosphorylated focal adhesion kinase then recruits phosphatidylinositol-3 kinase (PI3K), resulting in the activation of PI3K pathways (35). PI3Ks are members of a family of lipid kinases composed of a p85 regulatory subunit and a p110 catalytic subunit (28). Activation of this PI3K pathway leads to the generation of phosphoinositol-3,4-biphosphate and phosphatidylinositol-3,4,5-triphosphate (PIP_3). These messengers are involved in vesicular trafficking (43) and the rearrangement of cytoskeletal proteins such as actin (28). Interestingly, activated Rac1 and PI3K pathways are also required for the internalization of adenovirus (35).

Productive transduction by many viruses requires that virions gain access to the nucleus following infection. However, cytoskeletal network proteins such as actin and tubulin prevent free diffusion of large particles in the cytoplasm (54). These microtubules and microfilaments not only serve as barriers but also act as "highways" to facilitate the trafficking of these particles to specific destinations such as the nucleus or lysosomes. For example, nuclear targeting of adenovirus (49) has been shown to require functional microtubules and microfilaments (19, 34, 35, 57). Using Cy3-labeled AAV-2, we investigated the mechanisms of endocytosis and nuclear trafficking for this virus. Our results indicate that endocytosis of AAV-2 occurs through an αVβ5 integrin/Rac1-dependent mechanism and that subsequent trafficking of the virus to the nucleus requires activation of PI3K pathways as well as functional microtubules and microfilaments.

MATERIALS AND METHODS

Analysis of purity of rAAV stocks. The tgAAVCF vector, an AAV-2 vector encoding the cystic fibrosis transmembrane conductance regulator (CFTR) transgene, was produced and purified by Targeted Genetics (Seattle, Wash.) using column chromatography. tgAAVCF was free of detectable replication-competent adenovirus and replication-competent AAV (<3 IU/10^{10} DNase-resistant particles), bacteria, fungi, mycoplasmas, and endotoxin. To further assess the purity of the virus to be used for coupling to the Cy3 dye, decreasing

* Corresponding author. Mailing address: Department of Anatomy and Cell Biology, University of Iowa, College of Medicine, 51 Newton Rd., Room 1-111 BSB, Iowa City, IA 52242. Phone: (319) 335-7753. Fax: (319) 335-7198. E-mail: john-engelhardt@uiowa.edu.

amounts of tgAAVCF (from 20 to 1 μl) were electrophoresed on a 12% polyacrylamide–Tris–glycine gel (Novex); 50 ng of β-galactosidase protein (Sigma) was used as a reference standard. The gel was run for about 1.5 h at 140 V in 1× running buffer (5.8 M Tris, 28.8 M glycine, 0.05% [vol/vol] sodium dodecyl sulfate [SDS]). The gel was removed, washed for 10 min in 7.5% (vol/vol) acetic acid, then stained for 1 h with Sypro-Orange (Molecular Probes) and destained for 10 min in 7.5% acetic acid. The gel was scanned using a Storm Imager and then analyzed using Image Quant Software (Molecular Dynamics). Data analysis was performed to calculate the purity of virus based on the percentage of viral capsid proteins (VP1, VP2, and VP3) to total protein staining.

Cy3 labeling of rAAV and analysis in HeLa cells. Purified rAAV was dialyzed and concentrated in conjugation buffer (0.1 M sodium carbonate [pH 9.3]) using Centricon 30 ultrafilters (Millipore) prior to the labeling reaction. The lyophilized Cy3 dye was also dissolved in conjugation buffer. Briefly, samples of virus (5×10^{11} particles) were incubated for 30 min at room temperature with the *N*-hydroxysuccinimide (NHS)-ester carbocyanine (Cy3) dye in a reaction volume of 1 ml. The solutions were then transferred to dialysis chambers (10,000-molecular-weight cut-off; Gibco-BRL) and dialyzed for 24 h against two changes of buffer containing 20 mM HEPES (pH 7.5) and 150 mM NaCl. Lastly, the samples were dialyzed overnight in Dulbecco's modified Eagle's medium (DMEM) with no serum and concentrated in a Centricon 30. Dye-to-virus particle (D/P) ratios of the Cy3-labeled virus samples were calculated according to the manufacturer's instructions (Amersham Life Science) and were approximately equal to 1. The dialyzed Cy3-virus solution (Cy3AAV) was used directly for infecting HeLa cells (multiplicity of infection [MOI] of 10,000 DNA particles/cell) on glass slides at 4°C for 60 min (in the absence of serum). Following binding of the labeled virus at 4°C, slides were washed in serum-free medium twice and either fixed immediately for analysis or shifted to 37°C for continued infection in the presence of medium containing 10% serum. It should be noted that low-temperature incubation of HeLa cells resulted in subtle alterations in cell structure, as indicated by rounding of cells and cytoplasmic blebbing. However, these changes were independent of virus application.

Heparin competition assay. HeLa cells were incubated with CellTracker Green 5-chloromethylfluorescein diacetate (Molecular Probes) for 0.5 h at 37°C to permit visualization of subcellular compartments. Cells were then infected with Cy3-labeled rAAV at an MOI of 10,000 DNA particles/cell in the presence of increasing concentrations of heparin (40 μM, 200 μM, and 1 mM; Sigma) at 4°C for 60 min. After the incubation, cells were washed in phosphate-buffered saline (PBS) and fixed in 2% paraformaldehyde.

Immunocytochemistry. Cy3AAV-infected HeLa cells were incubated for 1 h at 4°C to allow virus binding. Cells were fixed in 100% methanol by incubating at −20°C for 10 min. After three washes in PBS, blocking was performed in 20% goat serum for 30 min. Samples were incubated in 1.5% goat serum–PBS containing 25 μg of primary B1 monoclonal anticap antibody (ARP Inc.; catalog no. 03-61058) per ml for 1 h at room temperature, followed by three washes with 1.5% goat serum–PBS. Fluorescein isothiocyanate (FITC)-labeled secondary antibody (anti-mouse immunoglobulin G [IgG]; Boehringer Mannheim Corp.) was added and incubated for another 30 min. After extensive washing in 1.5% goat serum–PBS, the slides were coverslipped with Citifluor mountant.

Preparation of Ad.N17Rac1 and Ad.CMVLacZ and Ad.K44Adynamin stocks. Three recombinant adenovirus vectors expressing either β-galactosidase (Ad.CMVLacZ) (20), a dominant negative mutant of Rac1 (Ad.N17Rac1) (32), or a dominant negative mutant of dynamin (Ad.K44Adynamin) (10, 27) were used for functional studies. Recombinant adenoviral stocks were generated as previously described (18) and stored in 10 mM Tris with 20% glycerol at −80°C. The particle titers of adenoviral stocks were determined by A_{260} readings and were typically 10^{13} DNA particles/ml. The functional titers of adenoviral stocks were determined by plaque titering on 293 cells and expression assays for encoded proteins. Typically the particle-to-plaque-forming unit ratio was equal to 25.

Morphologic assays to test involvement of αVβ5 integrin and Rac1 in rAAV endocytosis. Several assays were performed to assess the involvement of αVβ5 integrin and Rac1 in Cy3AAV endocytosis. These studies utilized an adenoviral vector encoding a dominant mutant to Rac1 (Ad.N17Rac1) or blocking antibodies to αVβ5 integrin. Affinity-purified mouse anti-human IgG αVβ5 integrin monoclonal antibody was obtained from Chemicon International (catalog no. MAB1961; Temecula, Calif.). This monoclonal antibody has been previously demonstrated to block vitronectin binding to αVβ5 receptors (62). Affinity-purified goat anti-mouse IgG control antibody was obtained from Boehringer Mannheim Biochemicals (catalog no. 605240; Indianapolis, Ind.). For blocking antibody experiments, HeLa cells were incubated with either anti-human αVβ5 or anti-mouse IgG at a final concentration of 2 μg/ml in the presence of Cy3AAV for 1 h at 4°C. For dominant inhibitor studies, cells were infected with either Ad.N17Rac1 or Ad.CMVLacZ at MOIs of 200 and 1,000 DNA particles/cell, respectively, for 48 h prior to Cy3AAV binding for 1 h at 4°C. Following viral binding at 4°C, samples were washed and either fixed immediately or incubated for an additional 10 to 120 min at 37°C. For blocking antibody experiments, Cy3AAV infections were performed in the continued presence of antibodies (2 μg/ml). The amount of membrane-bound and endocytosed Cy3AAV was determined as described below using computer-aided image analysis.

Wortmannin, nocodazole, and cytochalasin B assays. HeLa cells were treated with wortmannin (0.1 and 1 μM; Sigma), nocodazole (20 and 100 μM; Sigma), or cytochalasin B (5 or 20 μM) for 1 h at 37°C. After the slides were washed in DMEM, Cy3AAV was added to the cells (MOI of 10,000 particles/cell). Cells were then incubated at 4°C for 1 h, followed by washing and continued incubation in the presence of wortmannin, nocodazole, or cytochalasin B at 37°C for 2 h. Control cells were similarly infected with Cy3AAV but did not receive any inhibitor.

Rac1 activation assay. Rac1 activation assays were performed using a modified previously described protocol (23). pGEX-PBD (PBD encodes the p21 binding domain of Pak1, an effector molecule of activated Rac-1) was kindly provided by Richard Cerione (4). Glutathione-*S*-transferase (GST)-PBD fusion protein was purified from DL21 cells (Amersham Pharmacia Biotech, Piscataway, N.J.) transformed with pGEX-PBD. Bacteria were grown at 37°C to log phase and treated with 1 mM isopropyl-1-thio-β-D-galactopyranoside (IPTG) for 2 h. The cells were centrifuged, and the cell pellet was resuspended in lysis buffer (20 mM Tris-HCl [pH 7.5], 100 mM NaCl, 5 mM $MgCl_2$, 0.5% Nonidet P-40, 1 mM phenylmethylsulfonyl fluoride [PMSF], 10 μg of leupeptin per ml, and 10 μg of aprotinin per ml). Cells were then further lysed by three rounds of sonication (each lasting for 30 s). The lysate was subsequently centrifuged at 10,000 × *g* for 15 min, and the fusion proteins were isolated from the supernatant using a bulk GST purification kit (obtained from Amersham Pharmacia Biotech, Piscataway, N.J.). The purified protein appeared as a single band on sodium dodecyl sulfate-polyacrylamide gel electrophoresis (SDS-PAGE) with Coomassie blue staining. Protein concentrations were determined using the Bradford assay. For selective precipitation of GTP-bound Rac1, the GST-PBD fusion protein (50 μg) was first bound to agarose-conjugated anti-GST antibody (20 μg) (Santa Cruz Biotechnology, Inc, Santa Cruz, Calif.; catalog no. sc-138 AC) in 500 μl of lysis buffer at 4°C overnight. Subsequently, samples were centrifuged at 2,500 × *g* for 5 min and then washed three times with lysis buffer. These PBD-bound agarose beads were used for precipitation of GTP-bound Rac1 from virally infected HeLa cells as described below.

Confluent monolayers of HeLa cells were infected with tgAAVCF virus at an MOI of 5,000 DNA particles/cell and incubated at 37°C for 0, 5, and 15 min. Cells were harvested into lysis buffer (20 mM HEPES [pH 7.4], 0.5% NP-40, 10 mM $MgCl_2$, 10 mM β-glycerophosphate, 10% glycerol, 10 μg of leupeptin per ml, 10 μg of aprotinin per ml) at various time points by scraping. Precipitation of GTP-bound Rac1 was performed by the addition of 500 μg of HeLa cell lysate to GST-PBD-bound agarose beads for 2 h at 4°C. Samples were then spun at 2,500 × *g* for 5 min followed by three washes with lysis buffer. After boiling samples at 100°C for 5 min in SDS-PAGE sample buffer followed by centrifugation, samples were loaded onto SDS–12% PAGE for Western blotting against anti-Rac1 antibodies. Nitrocellulose filters were blocked (5% nonfat dry milk in 1× PBST) at 4°C overnight followed by incubation with rabbit polyclonal anti-Rac-1 antibody (Santa Cruz Biotechnologies) (0.2 μg/ml) diluted in blocking buffer for 1 h at 25°C. Subsequently, the filter was washed and incubated with peroxidase-conjugated anti-rabbit IgG (Boehringer Mannheim Biochemicals) at 0.4 μg/ml for 1 h at 25°C. The filters were finally washed and developed using a chemiluminescence luminol reagent (Santa Cruz Biotechnologies) and exposed to X-ray film. As a loading control, anti-GST (Santa Cruz Biotechnology; GST(B-14), catalog no. sc-138) antibody was also used to probe the filters.

PI3K activation assays. The PI3K activation assay was modified from a previously published protocol by Upstate Biotechnology (Lake Placid, N.Y.). Confluent monolayers of HeLa cells were infected with tgAAVCF virus at an MOI of 5,000 DNA particles/cell and incubated at 37°C for 0, 5, or 15 min. HeLa cells were lysed in a lysis buffer containing 1% NP-40, 10 mM NaF, 2 mM sodium pyrophosphate, 0.4 mM Na_3VO_4, 0.05 M Tris (pH 7.4), and 0.15 M NaCl, with protease inhibitor cocktail (100 μg of pepstatin, 10 μg of leupeptin, and 50 μg of aprotinin per ml plus 0.5 M PMSF). Cells were then further lysed by four rounds of sonication (each lasting for 30 s). Cellular debris were removed by centrifugation at 10,000 × *g* for 10 min. Protein concentrations were determined using the Bradford assay. The catalytic complex of PI3K was immunoprecipitated using anti-PI3K p85 antibody (Santa Cruz) conjugated to Gamma Bind Plus Sepharose (Amersham-Pharmacia) at 4°C overnight. The beads were washed with PBS three times and incubated with 500 μg of cellular lysate at 4°C overnight. Samples were washed three times with buffer 1 (1% NP-40 and 100 μM Na_3VO_4), three times with buffer 2 (100 mM Tris HCl [pH 7.5], 500 mM LiCl, 100 mM Na_3VO_4), and twice with buffer 3 (10 mM Tris-HCl [pH 7.5], 100 mM NaCl, 1 mM EDTA, 100 μM Na_3VO_4), and then resuspended in 50 μl of buffer 3. A 10-μl amount of each sample was used for Western blotting against anti-p85 antibody to ensure equivalent levels of immunoprecipitation of the PI3K complex. PI3K assays were performed using sonicated L-α-phosphatidylinositol (Avanti Lipids, Alabaster, Ala.) as the substrate. L-α-Phosphatidylinositol was dissolved in 10 mM Tris (pH 7.5) with 1 mM EGTA and added to the cellular extracts in the presence of 14 mM $MgCl_2$ for 5 min at room temperature. Then 30 μCi of [γ-^{32}P]ATP (Amersham-Pharmacia) and 63 μM ATP were mixed with the samples and allowed to react for 5 to 15 min at room temperature. The desired product (PIP_3) was extracted by addition of chloroform-methanol (1:1) along with 160 μM HCl. The samples were dried under nitrogen flow and then resuspended in chloroform-methanol (1:1) prior to analysis by thin-layer chromatography (TLC) using silica gel coated with 10% potassium oxalate. Chloroform-methanol-water-ammonium hydroxide (60:47:11.3:2) was the separation solvent. The production of PIP_3 was quantitated using a phosphoimager and exposed to X-ray film.

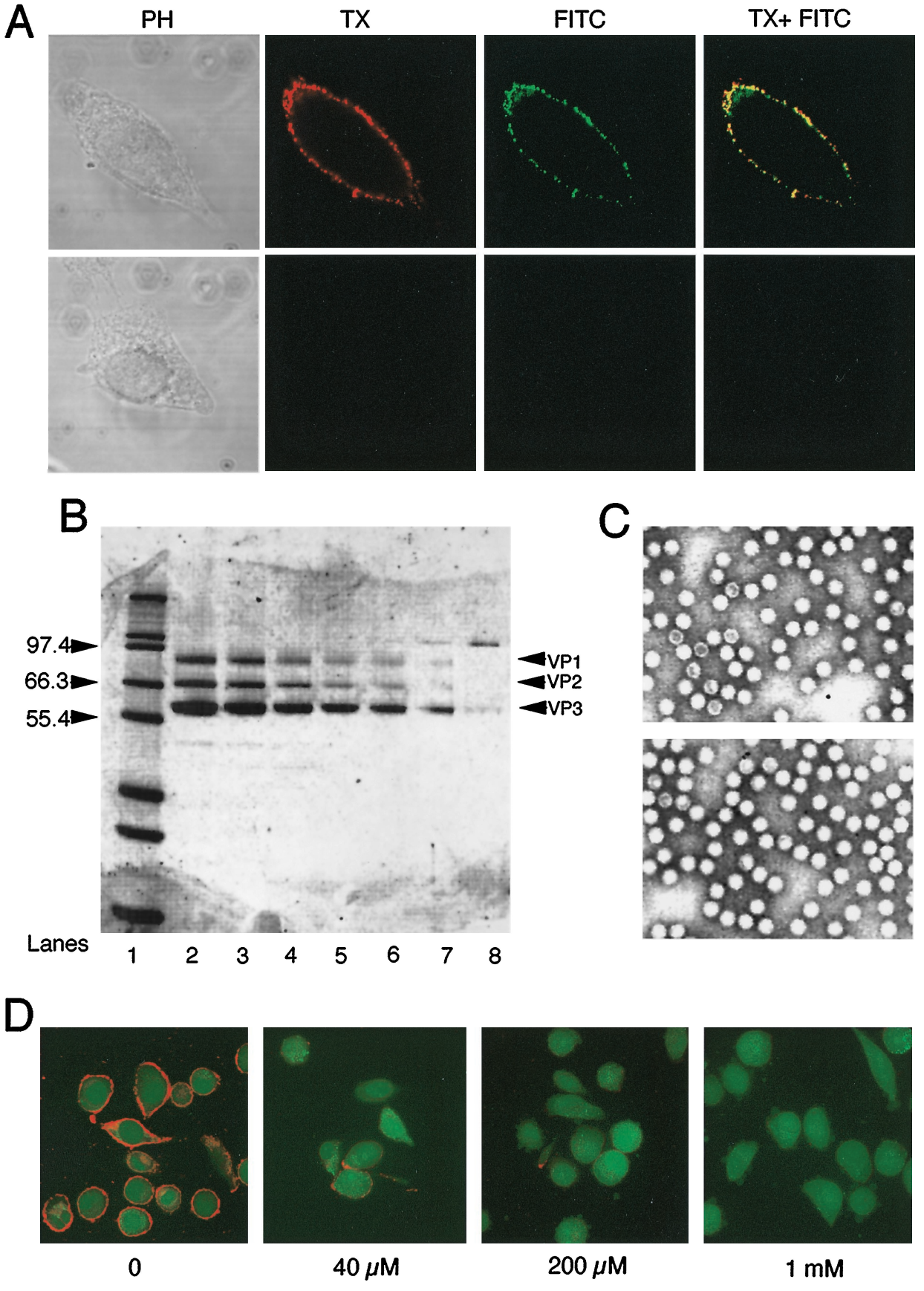
A
PH
TX
FITC
TX+ FITC
B
97.4
66.3
55.4
VP1
VP2
VP3
Lanes
1 2 3 4 5 6 7 8
C
D
0
40 μM
200 μM
1 mM

Hirt DNA preparations, subcellular fractionation, and Southern blotting for viral DNA. HeLa cells were treated with inhibitors (nocodazole, cytochalasin B, wortmannin, anti-mouse IgG, and integrin blocking antibody as described above) for 1 h at 37°C. For studies evaluating Rac1 involvement, cells were infected with Ad.N17Rac1 or Ad.CMVLacZ at an MOI of 1,000 particles/cell 48 h prior to rAAV infection. Following the above treatments, cells were then washed and incubated with AV.GFP3ori virus (15) at an MOI of 1,000 DNA particles/cell for 1 h at 4°C. Following binding, cells were washed with PBS three times and either harvested directly by scraping or trypsinization or shifted to 37°C for 2 h to promote internalization of virus prior to harvesting. Cell harvesting by trypsinization following by washing in PBS was used to remove extracellular bound virus. Extraction of low-molecular-weight Hirt DNA (viral DNA) and Southern blotting were performed according to protocols described previously (25, 52). In addition to the above methods for determining the extent of internalized and external membrane-bound virus, nuclear and cytoplasmic extracts were prepared to evaluate nuclear accumulation of virus following treatment with nocodazole, cytochalasin B, and wortmannin. Cellular and nuclear fractions were prepared according to a modified procedure of Andrew and Faller (3). Hirt DNA extractions from each of these subcellular fractions were performed as described above to recover viral DNA.

Image analysis. Phase-contrast and Texas red channels were superimposed to mark the nuclear and cell boundaries using the Volume Trace Motif Version 3.1 program (The University of Iowa Image Analysis Facility, Iowa City, Iowa). A histogram equalization was performed on each image to maximize the contrast for boundary visualization. Viral particle distributions in the nucleus and in the cytoplasm were assessed using the tal_program (Randall Frank, Brainvox, Human Neuroanatomy and Neuroimaging Lab, Department of Neurology, University of Iowa). Cy3 pixels (AAV) were visualized as white pixels (255 = absolute value for a white pixel) by setting the threshold to the maximum gray level value of background pixels (tal_threshold). Using tal_stat, the pixel mean for a region was determined. The number of white pixels was calculated from the formula of pixel mean = [(number of white pixels × 255) + (number of black pixels × 0)]/(total pixels). The numbers of regional pixels as membrane bound versus intracellular or cytoplasmic versus nuclear were divided by the number of total pixels in order to determine the regional percentages of Cy3AAV. It must be acknowledged that due to our sampling of nuclear cross-sections, it is possible that we have underestimated the extent of nonnuclear AAV particles. Nevertheless, comparative analysis between samples using this method of evaluation is informative. Three-dimensional (3-D) image reconstruction was used to evaluate whether Cy3-labeled capsid proteins entered the nucleus. In these studies the nucleus and cytoplasm of individual 0.5-μm phase-contrast confocal scans were pseudocolored in blue and green, respectively. The individual confocal layers (both phase-contrast and red channel) were then reconstructed into a 3-D image using the Voxblast program developed by the Image Analysis Core Facility at the University of Iowa.

Transmission electron microscopy. We used 300-mesh copper Formvar-coated grids (90 nm) treated with 0.5% polyvinyl formaldehyde in ethylene dichloride. Samples were placed on coated grids, stained in 1% ammonium molybdate for 30 s, and then examined using a Hitachi H-7000 transmission electron microscope.

RESULTS

Functional characterization of Cy3-labeled rAAV. The bifunctional NHS-ester carbocyanine-Cy3 was conjugated to highly purified rAAV virions as explained in Materials and Methods. To confirm that Cy3 was labeling capsid proteins and not other minor impurities in the virus samples, HeLa cells infected with Cy3-labeled particles were stained with a B1 antibody developed against the three AAV-2 capsid proteins. Results from this study confirmed that all Cy3-labeled particles colocalized with AAV capsid proteins on the surfaces of HeLa cells following binding at 4°C for 1 h (Fig. 1A). These results are consistent with the estimated purity (>99%) of viral stocks used in labeling reactions (Fig. 1B). As seen in Fig. 1B (lanes 2 to 7), only three bands, VP1, VP2, and VP3, were detected on SDS-PAGE. In order to determine if the conjugation reaction had altered the capsid structure of rAAV, both the labeled (Cy3AAV) and unlabeled (AAV) virus samples were examined by transmission electron microscopy (Fig. 1C). No alterations were detected in the capsid structure of rAAV after the labeling reaction. Additionally, to evaluate whether Cy3 labeling decreased the functional properties of rAAV, replication center assays (50) were performed on labeled and mock-labeled virus. The particle-to-infectious unit ratio was approximately 1,000 in both cases and was not altered by the presence of Cy3 (data not shown).

To characterize the binding properties of Cy3AAV, heparin competition assays were performed (Fig. 1D). Previously, heparin has been used as a specific competitor of AAV-2 binding to HeLa cells by blocking viral binding to its receptor, HSPG (56). As seen in Fig. 1D, increasing concentrations of heparin competed with Cy3-labeled rAAV for binding to HeLa cells in a dose-dependent fashion. Although the majority of AAV-2 binding was competitively inhibited with 40 μM heparin, some residual binding of rAAV was still evident even with 1 mM heparin (Fig. 1D). Since other types of rAAV coreceptors have been reported (47, 55), this residual binding could be due to the presence of rAAV receptors other than HSPG on the cell surface.

To examine the mechanisms of AAV endocytosis and nuclear trafficking, we first sought to determine the time course of AAV movement from the membrane to the nucleus. Following binding of Cy3-labeled virus to HeLa cells at 4°C for 1 h (Fig. 2A), 12 and 51% of the total Cy3AAV particles were localized to nuclei within 0.5 and 1 h at 37°C, respectively (Fig. 2B and C). By 2 h at 37°C, the majority of virus particles were localized to the nucleus (82%), and by 3 h nearly all virions were nucleus associated (93%), as determined by morphometric image analysis (Fig. 2J). For this reason, subsequent experiments examining endocytosis and nuclear trafficking of virus were performed at 1 and 2 h of incubation at 37°C. 3-D image reconstruction was also used to examine whether Cy3-labeled capsid proteins entered the nucleus. Results of this analysis are depicted in Fig. 2F to I and clearly demonstrate that by 2 h postinfection, a fraction of nucleus-associated virus had localized within the nucleus.

Endocytosis of rAAV is inhibited by blocking antibodies against integrin αVβ5. It has been reported that efficient AAV-2 infection requires coreceptors such as human fibroblast growth factor receptor 1 (47) or αVβ5 integrins (55). In order to test whether αVβ5 integrins mediate rAAV binding and/or endocytosis in HeLa cells, infections with Cy3AAV were performed in the presence of a blocking anti-human αVβ5 integrin monoclonal antibody or control anti-mouse IgG. As seen in Fig. 3, neither anti-human αVβ5 integrin antibodies (panel E) nor control anti-mouse IgG (panel C) interfered with the binding of Cy3AAV to HeLa cells, since they were indistinguishable from untreated controls (panel A). These findings suggest that αVβ5 integrin is not required for binding of AAV-2 to HeLa cells. However, when the temperature was shifted to 37°C for 45 min to initiate endocytosis, uptake of Cy3AAV was inhibited only in cells treated with

FIG. 1. Cy3 conjugation to AAV capsids. HeLa cells were infected with rAAV labeled with Cy3 as explained in Materials and Methods. (A) Fluorescent colocalization of Cy3AAV (left panel in red) with AAV capsid proteins stained with FITC-labeled anti-cap B1 antibody (center panel in green). The two channels are superimposed in the right panel, demonstrating colocalization of Cy3AAV and capsid proteins (in yellow). SDS-PAGE analysis, following staining with Sypro-Orange, was used to evaluate the purity of the rAAV preparation used for Cy3 labeling (B). Lane 1 contains molecular size markers, and the sizes (in kilodaltons) are given to the left of the gel. Various amounts of rAAV from 20 to 1 μl were loaded onto lanes 2 to 7 in a 12% polyacrylamide–Tris–glycine gel (Novex). The locations of capsid proteins VP-1, -2, and -3 are marked to the right of the gel. Lane 8 contains 50 ng of β-galactosidase protein as a reference. (C) Ultrastructure of unlabeled (upper panel) and Cy3-conjugated AAV (lower panel) by transmission electron microscopy. The binding of Cy3-labeled AAV to its receptor on HeLa cells was tested for competition by increasing amounts of heparin (D). Numbers below each panel indicate the doses of heparin used in these assays.

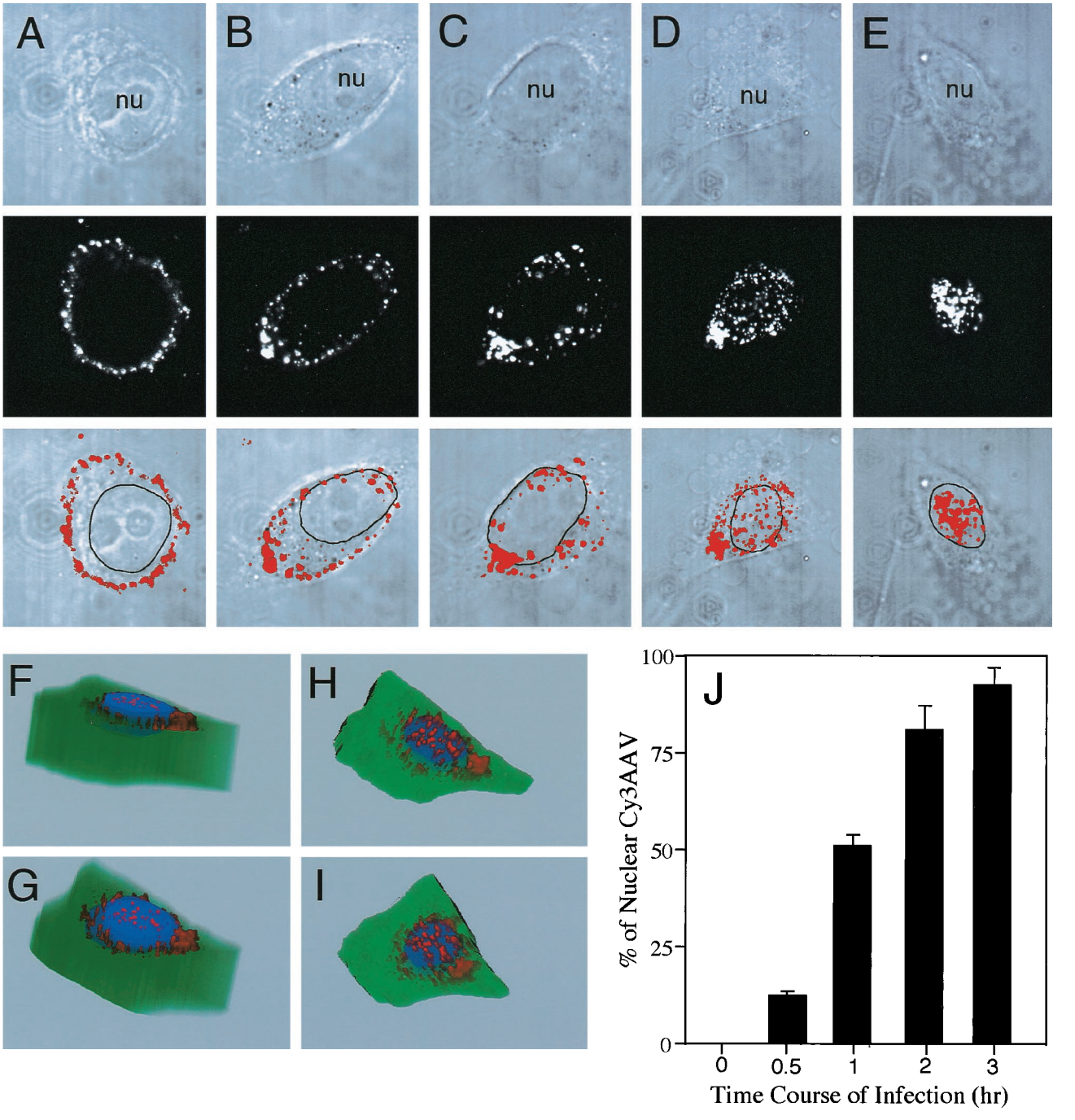

FIG. 2. Time course of AAV translocation to the nucleus. HeLa cells were incubated with Cy3AAV at 4°C for 1 h to promote virus binding. Following binding, cells were either immediately washed and fixed (A) or washed and then shifted to 37°C for 0.5 (B), 1 (C), 2 (D), or 3 (E) h prior to fixation. Cells were then analyzed by confocal fluorescent microscopy. Each image is a stack of three consecutive 0.5-μm layers, with each panel representing confocal phase contrast (top), gray scale Cy3 (middle), and superimposed images (bottom). The nucleus (nu) of each cell is marked for clarity. 3-D reconstructed images were generated from 25 (F and G) or 5 (H and I) consecutive 0.5-μm confocal layers obtained after both phase-contrast and red channel scans from a cell infected for 2 h at 37°C. Cellular architecture was generated from the individual phase-contrast confocal images, with the nucleus pseudocolored in blue and the cytoplasm in green. The same cell is represented in each panel with a different angle of rotation. The percentage of nucleus-associated Cy3AAV particles was determined using morphometric image analysis as explained in Materials and Methods ($n = 7$ cells analyzed for each time point) and is graphically represented in panel J. Values in panel J are the mean ± standard error of the mean (SEM) percentage of particles associated with the nucleus for each time point.

anti-human αVβ5 integrin antibody (panel F). The anti-human αVβ5 integrin antibody appeared to prevent endocytosis, leaving virus at the membrane. No effect on Cy3AAV endocytosis was seen in cells treated with anti-mouse IgG (panel D), which were indistinguishable from untreated cells (panel B). These results suggested that αVβ5 integrin is involved in endocytosis of rAAV virus in this HeLa cell model.

In order to conclusively address whether AAV was on the external or internal face of the membrane following treatment with integrin-blocking antibody, the extent of trypsin-resistant

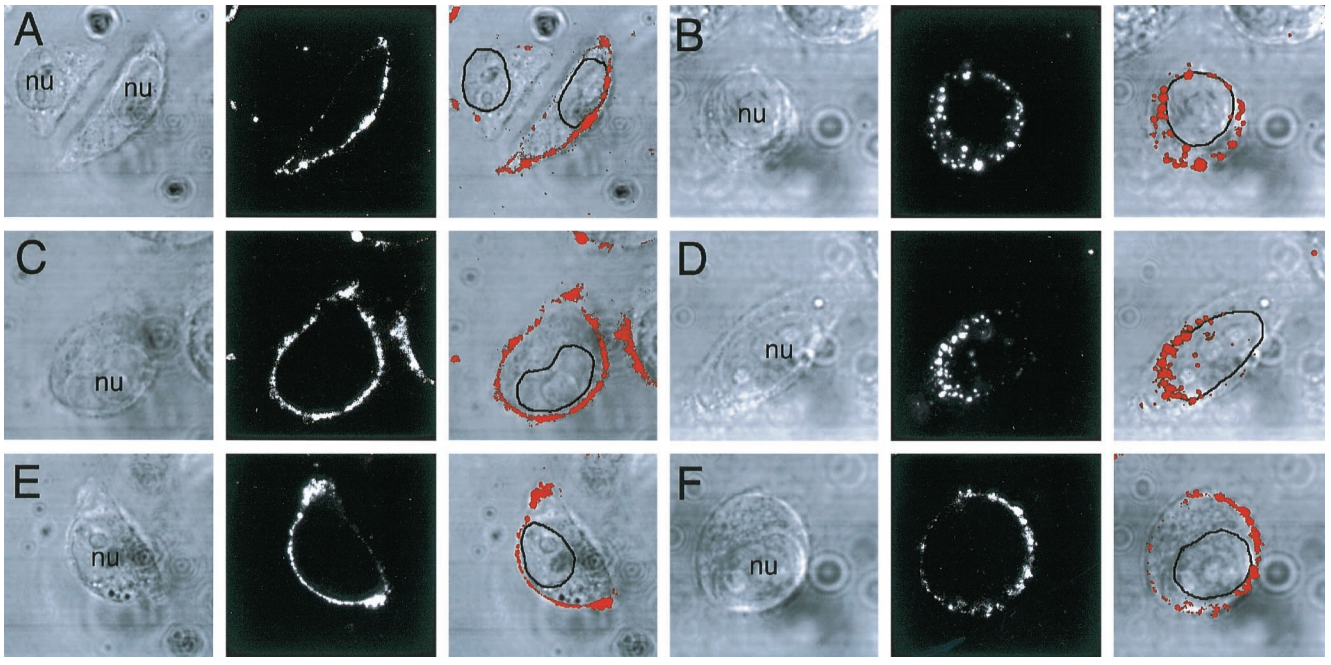

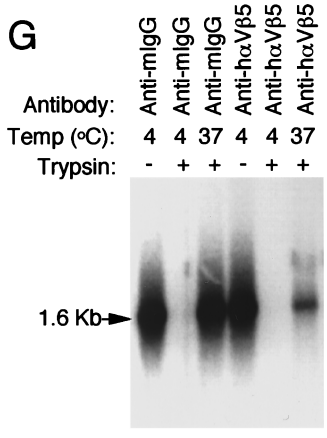

FIG. 3. αVβ5 integrin is required for the endocytosis of AAV-2 virus. Cy3AAV was incubated alone (A and B) or in the presence of control anti-mouse IgG antibody (C and D) or anti-human αVβ5 integrin-blocking antibody (E and F) at 4°C for 1 h. Cells were then either washed and fixed immediately (A, C, and E) or washed and incubated for an additional 45 min at 37°C (B, D, and F). Representative confocal photomicrographs are shown for each condition. Each of the panels shows the confocal phase-contrast image (left), gray scale stack of Cy3AAV images (middle), and superimposed images (right). Each confocal image is a stack of six consecutive 0.5-μm layers that intersect the nucleus. The nucleus (nu) of each cell is marked for clarity. Southern blotting of Hirt DNA isolated from rAAV-infected cells was performed as an alternative approach to evaluate rAAV endocytosis in cells treated with anti-mouse IgG or anti-human αVβ5 integrin (G). HeLa cells were infected with unlabeled AV.GFP3ori virus (MOI of 1,000 DNA particles/cell) for 1 h at 4°C, washed, and shifted to 37°C for 2 h. Cells were harvested by either direct scraping to determine viral binding (− trypsin) or by trypsinization to remove extracellular virus (+ trypsin). Hirt DNA was prepared from cells treated with the various conditions, and Southern blots were hybridized with P^{32}-labeled EGFP cDNA probe. Single-stranded rAAV genomes are marked by a 1.6-kb hybridizing band.

(internalized) virus was analyzed following infection under the various conditions. Southern blotting analysis of Hirt DNA isolated from cells treated with either anti-mouse IgG or αVβ5 integrin-blocking antibody indicated no effects on viral binding at 4°C compared to the untreated cells (Fig. 3G). In contrast, when cells were shifted to 37°C for 2 h following viral binding, a significant reduction in intracellular, trypsin-resistant viral DNA was seen only in cells treated with αVβ5 integrin-blocking antibody, but not with control anti-IgG. These findings substantiate earlier morphologic observations in supporting a role for αVβ5 integrin in the early steps of AAV-2 endocytosis.

Endocytosis of AAV-2 is blocked by expression of a dominant negative mutant form of Rac1 (N17Rac1). Integrins have been demonstrated to associate with small intracellular signaling molecules, such as Rho, Rac, and Cdc42 GTPases (42, 45). The Rac GTP-binding protein has been shown to control mitogenic and oncogenic signals through NADPH-oxidase superoxide production (26, 44). Interestingly, reactive oxygen species have been implicated in augmenting rAAV transduction by an as yet unknown mechanism (53). Given the correlation between reactive oxygen species involvement in rAAV-2 transduction and results demonstrating a role for integrins in rAAV endocytosis, we hypothesized that Rac1 and αVβ5 integrin may interact in the endocytic events controlling AAV-2 infection.

In order to test this hypothesis, recombinant adenovirus expressing dominant negative Rac1 (Ad.N17Rac1) (32) was used to inhibit Rac1 activity in HeLa cells, and the effects on AAV endocytosis were evaluated. As a negative control, HeLa cells were also infected with adenovirus expressing the *lacZ* gene (Ad.CMVLacZ). At 48 h after adenoviral infection with either Ad.N17Rac1 or Ad.CMVLacZ, HeLa cells were infected with Cy3AAV virus. The endocytic process was followed for 10 min to 2 h (only the 45-min time point is shown in Fig. 4). The total amount of endocytosed Cy3AAV was then calculated in N17Rac1- and Ad.CMVLacZ-infected cells as described in Materials and Methods (Fig. 4J). Binding studies performed at 4°C for 1 h demonstrated that neither Ad.CMVLacZ (Fig. 4D) nor Ad.N17Rac1 (Fig. 4G) infection altered the efficiency of viral binding in comparison to uninfected controls (Fig. 4A). However, 60% (Fig. 4H) and 99% (Fig. 4I) reductions in the number of endocytosed Cy3AAV particles at 45 min post-AAV infection were observed when cells were in-

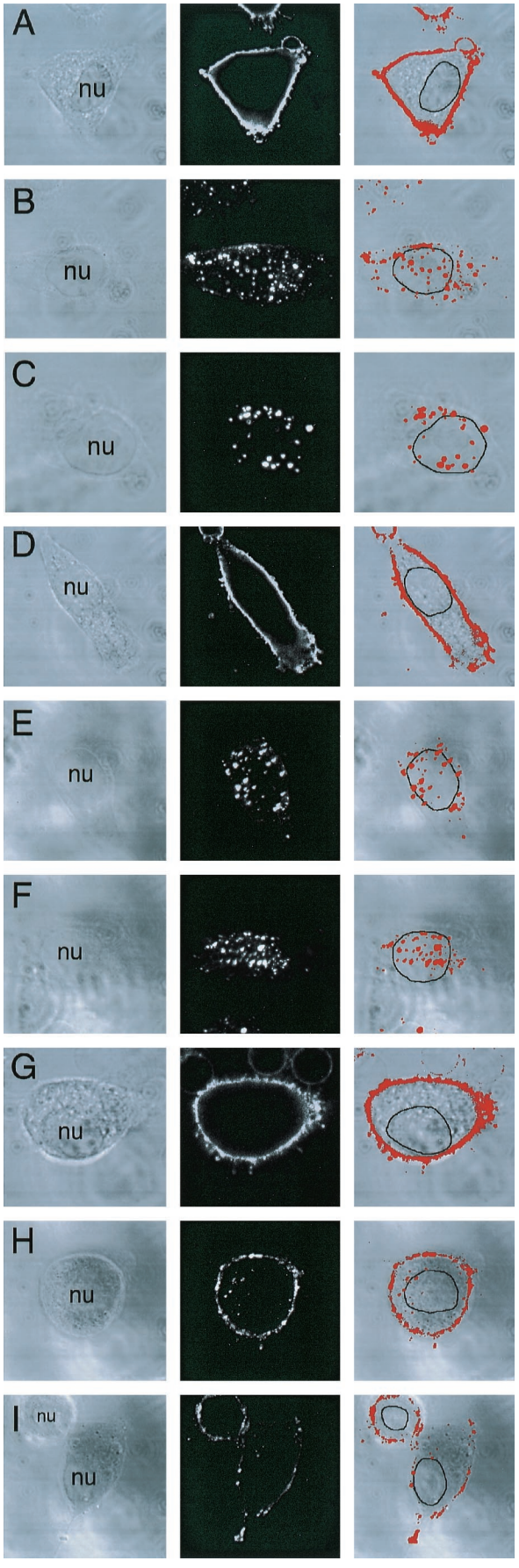

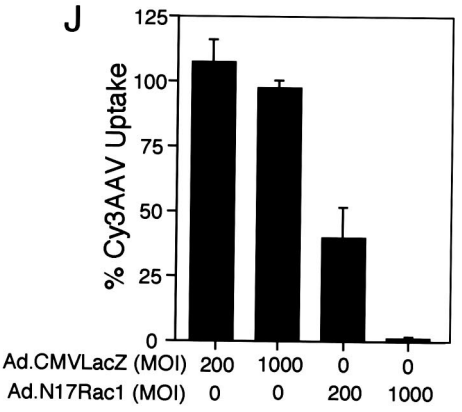

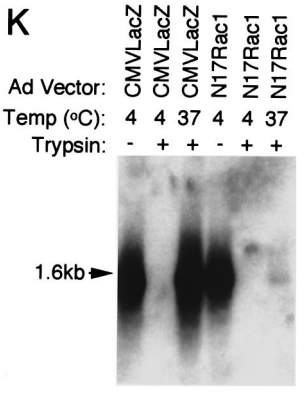

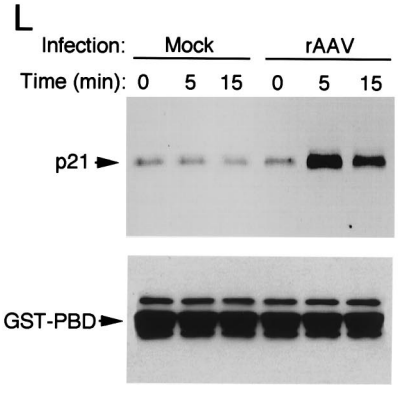

FIG. 4. AAV endocytosis requires Rac1 activation. A dominant inhibitor of Rac1 (N17Rac1) was used to evaluate the involvement of the small GTPase Rac1 in AAV endocytosis. HeLa cells were either uninfected (A to C) or infected with Ad.CMVLacZ (D to F) or Ad.N17Rac1 (G to I) virus at an MOI of 1,000 (D, F, G, and I) or 200 (E and H) particles/cell 48 h prior to incubation with Cy3AAV at 4°C for 1 h. Following incubation with Cy3AAV, cells were either washed and immediately fixed to examine viral binding (A, D, and G) or shifted to at 37°C for 45 min to examine endocytosis (B, C, E, F, H, and I). Representative confocal photomicrographs are given for each condition, representing six 0.5-μm stacked layers that intersect the nucleus. Each of the panels shows the confocal phase contrast image (left), gray scale stack of Cy3AAV images (middle), and superimposed images (right). The nucleus (nu) of each cell is marked for clarity. Panel J represents the mean percentage ± SEM (n = 7) of Cy3AAV particles internalized within a 45-min time period for each condition, as determined by computer-aided image analysis. Southern blotting of Hirt DNA isolated from rAAV-infected cells was performed as an alternative approach to evaluate rAAV endocytosis in Ad.N17Rac1- and Ad.CMVLacZ-infected (1,000 DNA particles/cell) HeLa cells (K). At 48 h following adenoviral infection, HeLa cells were infected with unlabeled AV.GFP3ori virus (MOI of 1,000 DNA particles/cell) for 1 h at 4°C, washed, and either harvested directly or shifted to 37°C for 2 h prior to harvesting. Cells were harvested by either direct scraping to determine viral binding (− trypsin) or by trypsinization to remove extracellular virus (+ trypsin).

fected with adenovirus expressing N17Rac1 at MOIs of 200 and 1,000, respectively. The majority of Cy3AAV particles appeared to remain associated with the cell surface membrane and were not endocytosed. In contrast, no reduction in Cy3AAV endocytosis was seen when cells were infected with Ad.CMVLacZ virus (Fig. 4E and F) compared to cells not infected with adenovirus (Fig. 4B and C). Interestingly, at high titers of Ad.N17Rac1, the number of AAV particles which remained bound to the surface membrane was significantly reduced. Given the fact that 4°C binding was unaffected by infection with Ad.N17Rac1 or Ad.CMVLacZ, we reasoned that virus must be diffusing away from the membrane during the 45-min 37°C incubation period. In fact, with prolonged 2-h incubations at 37°C, no virus remained in association with Ad.N17Rac1-infected cells (data not shown). In contrast, nuclear accumulation (and endocytosis) of Cy3-rAAV at the same prolonged incubation times in Ad.CMVLacZ-infected cells was indistinguishable from that in uninfected controls (data not shown).

In order to more conclusively address whether virus remained on the external face of the membrane in N17Rac1-expressing cells, we tested the trypsin sensitivity of virus following 4°C binding (1 h) and 37°C infection for 2 h using Hirt Southern blot analysis for viral DNA. As seen in Fig. 4K, N17Rac1 (but not *lacZ*) expression inhibited endocytosis of rAAV, as determined by the extent of trypsin-resistant intracellular viral genomes. These studies also demonstrated a lack of effect on viral binding at 4°C with either N17Rac1 or *lacZ* transgenes.

Based on the morphologic and molecular findings that AAV-2 endocytosis required functional Rac1, we next sought to evaluate whether Rac1 was directly activated by AAV-2 infection. These studies utilized a functional assay developed by Glaven and colleagues to detect the abundance of GTP-bound Rac1 with a GST-PBD fusion protein (23). As described in Materials and Methods, PBD encodes the p21 binding domain of Pak1 (an effector molecule of activated Rac1) and was used to selectively precipitate GTP-bound Rac1 (the active form). The abundance of GTP-bound Rac1 was then directly assessed by Western blot using anti-Rac1 antibodies. Extracts from HeLa cells infected with rAAV for 0 to 15 min were assayed to determine the level of Rac1 activity. As shown in Fig. 4L, the level of GTP-bound Rac1 increased significantly by 5 min postinfection with rAAV in comparison to mock-infected controls treated with vehicle alone. These results demonstrate that AAV-2 infection leads to activation of Rac1.

Efficient rAAV trafficking requires PI3K activation. Endocytosis and sorting of integrin-linked receptors have been previously suggested to require PI3K activity (41). For example, following endocytosis of vitronectin, inhibition of PI3K prevents vesicle sorting and movement to lysosomes (37). We hypothesized that the activation of Rac1 during endocytosis might be critical for signaling PI3K to initiate intracellular movement of endocytosed virus to the nucleus. Direct interactions between small GTP-binding proteins (i.e., Rac1, Rho, and Ccd42) and PI3K have also been reported (8, 59). For adenovirus, PI3K pathways also appear to be critical for viral entry and endocytosis (35). In addition, given the evolutionary

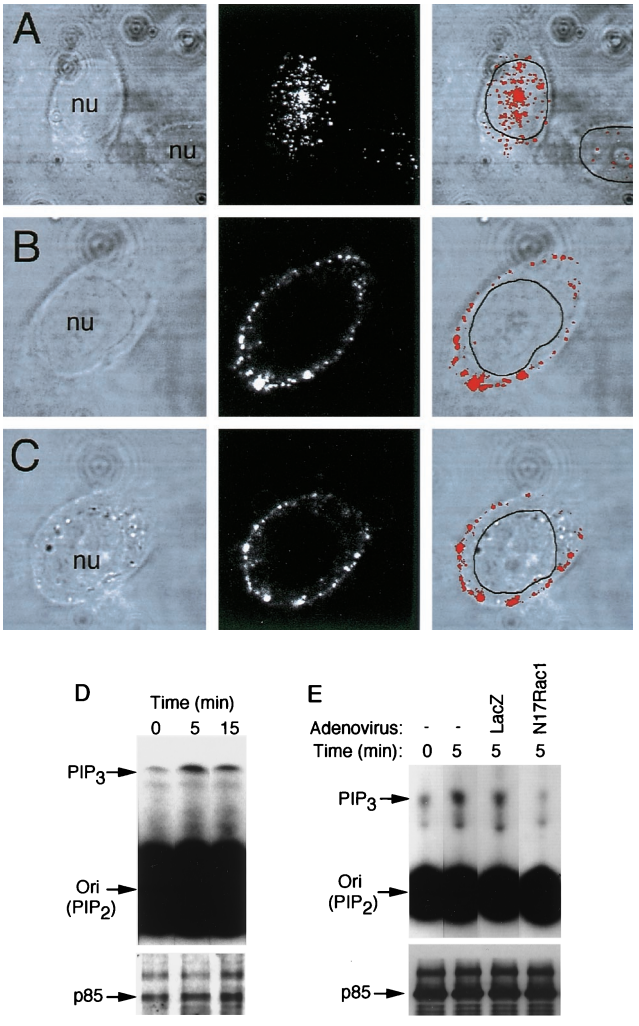

FIG. 5. Trafficking of Cy3AAV to the nucleus is sensitive to wortmannin treatment. HeLa cells were either untreated (A) or treated with 0.1 μM (B) or 1 μM (C) wortmannin for 1 h at 37°C prior to infection with Cy3AAV. Following wortmannin treatment, Cy3AAV was bound to cells for 1 h at 4°C, then the cells were washed of excess virus and incubated at 37°C for an additional 2 h in the continued presence of wortmannin. Representative confocal photomicrographs are given for each condition, each representing six 0.5-μm stacked layers that intersect the nucleus. Each panel illustrates the confocal phase contrast (left), gray scale stack of Cy3AAV images (middle), and superimposed images (right). The nucleus (nu) of each cell is marked for clarity. The effect of rAAV infection on PI3K activation was evaluated as described in Materials and Methods (D and E). Cells were infected with unlabeled tgAAVCF virus at an MOI of 5,000 DNA particles/cell for 0, 5, and 15 min at 37°C. The PI3K complex was immunoprecipitated from cell lysates and assayed in the presence of [γ-^{32}P]ATP and L-α-phosphatidylinositol followed by TLC and autoradiography (D, top). Faster migrating bands above the origin of migration (ori) indicate the product (PIP_3). Western blot analysis was also performed using anti-PI3K p85 antibody, which indicates that equal amounts of PI3K complex were used for each reaction (lower panel of D). To evaluate whether functional Rac1 was necessary for PI3K activation, cells were infected with either Ad.N17Rac1 or Ad.CMVLacZ virus at an MOI of 1,000 particles/cell for 48 h prior to assaying PI3K activity (E). Conditions for infection and times of harvest are marked above each lane of the TLC autoradiogram. The bottom panel is a Western blot using anti-PI3K p85 antibody.

Hirt DNA was prepared from the various conditions, and Southern blots were hybridized with a ^{32}P-labeled EGFP cDNA probe. Single-stranded rAAV genomes are marked by a 1.6-kb hybridizing band. Rac1 activation assays were performed as described in Materials and Methods. A Western blot detecting GST-PBD-precipitated GTP-bound Rac1 is given in panel L. Cells were infected with unlabeled tgAAVCF virus (MOI of 5,000 DNA particles/cell) or mock infected with vehicle alone for the exposure times indicated above each lane, then 500 μg of HeLa cell lysate from each condition was precipitated with GST-PBD and evaluated by Western blot against anti-Rac1 antibodies. The p21 band marked by an arrow is Rac1. The filters were also probed with anti-GST antibodies as a loading control. The position of GST-PBD protein is marked by an arrow below the Rac1 Western blot.

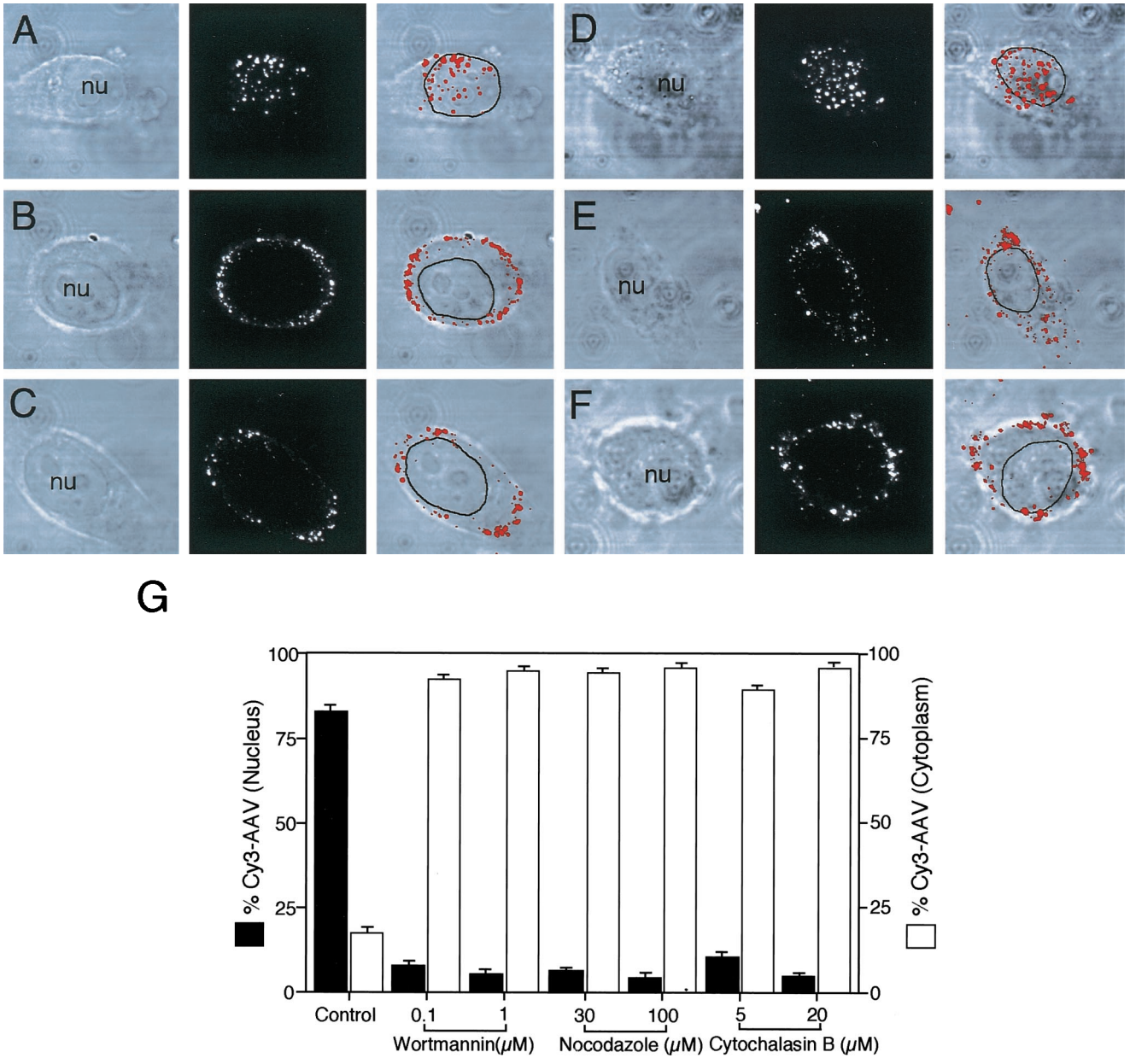

FIG. 6. Nocodazole and cytochalasin B treatment reduces nuclear targeting of Cy3AAV. HeLa cells were either untreated (A and D) or treated with 30 μM nocodazole (B), 100 μM nocodazole (C), 5 μM cytochalasin B (E), or 20 μM cytochalasin B (F) for 1 h at 37°C prior to infection with Cy3AAV. Following nocodazole and cytochalasin B treatment, Cy3AAV was bound to cells for 1 h at 4°C, and the cells were then washed of excess virus and incubated at 37°C for an additional 2 h in the continued presence of inhibitor. Representative confocal photomicrographs are given for each condition, each representing six 0.5-μm stacked layers that intersect the nucleus. Each of the panels shows the confocal phase contrast (left), gray scale stack of Cy3AAV images (middle), and superimposed images (right). The nucleus (nu) of each cell is marked for clarity. Quantitative analysis of AAV nuclear trafficking is shown in panel G. The percentages of cytoplasmic and nuclear associated Cy3AAV particles were quantified by morphometric image analysis, as explained in Materials and Methods, following treatment of cells with various chemical agents. Solid bars indicate nucleus-associated Cy3AAV, while open bars indicate cytoplasmic Cy3AAV particles. Values are the mean ± SEM of 10 cells quantified for each condition.

similarities between the shared αVβ5 integrin coreceptor of adenovirus and AAV (55) and the fact that both viruses appear to be endocytosed through clathrin-coated pits (61), we hypothesized that PI3K pathways might also be involved in AAV-2 endocytosis.

In order to determine whether the PI3K pathway is also important for the uptake of rAAV virus, cells were treated with the PI3K inhibitor wortmannin at increasing concentrations prior to the infection (Fig. 5A to C). The results indicate a significant reduction in Cy3AAV movement to the nucleus in the presence of wortmannin. Although a fraction of Cy3AAV particles remained on the cell surface membrane, the majority appeared to be trapped within the cytoplasm or just below the cell membrane. Only 7.4 and 5% of the virus particles were nucleus associated at concentrations of 0.1 and 1 μM wortmannin, respectively (Fig. 5B and C). This is contrasted to control samples not treated with wortmannin, for which 80% of viral particles were either in the nucleus or nucleus associ-

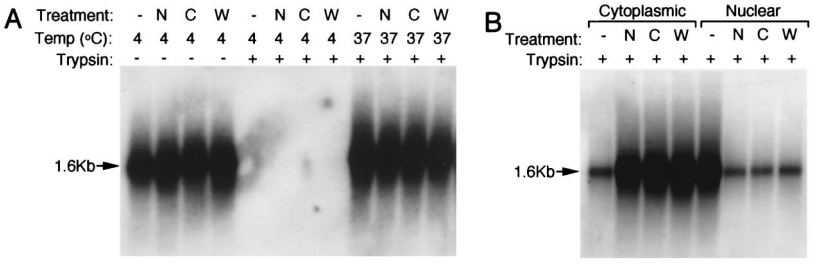

FIG. 7. Wortmannin, nocodazole, and cytochalasin B inhibit intracellular transport of AAV-2 to the nucleus but not endocytosis. HeLa cells were infected with unlabeled AV.GFP3ori virus (MOI of 1,000 DNA particles/cell) following treatment with wortmannin (W), nocodazole (N), or cytochalasin B (C). Protocols for chemical treatment were as described in Materials and Methods. Cells were infected for 1 h at 4°C, washed, and shifted to 37°C for 2 h. To determine the extent of viral endocytosis, cells were harvested after both 4 and 37°C incubation by either direct scraping to determine viral binding (− trypsin) or by trypsinization to remove extracellular virus (+ trypsin) (A). Alternatively, following 37°C incubations, cells were harvested by trypsinization and washed, and cytoplasmic and nuclear fractions were purified (B). Hirt DNA was prepared from cells or subcellular fractions following the various treatment conditions (as indicated above each lane), and Southern blots were hybridized with ^{32}P-labeled EGFP cDNA probe. Single-stranded rAAV genomes are marked by a 1.6-kb hybridizing band.

ated by 2 h postinfection (Fig. 5A). These results are somewhat different than those reported for adenovirus in that wortmannin appeared to block endocytosis of adenovirus, while with AAV the wortmannin-sensitive block appears to involve movement of AAV to the nucleus at a postendocytic level.

Given the apparent involvement of PI3K in nuclear trafficking of AAV-2, we asked whether PI3K activity was stimulated directly by AAV-2 infection. As shown in Fig. 5D, PI3K activity increased following rAAV infection of HeLa cells, with a maximal increase by 5 min postinfection, which declined slightly by 15 min. This time course was similar to that found for Rac1 activation. Western blot analysis for p85 (Fig. 5D) confirmed that equal amounts of the PI3K complex were added to each reaction. The results support the hypothesis that AAV endocytosis activates a PI3K pathway in Hela cells. Of particular interest for elucidating the mechanisms of AAV-2 endocytosis was the determination of whether PI3K activation was proximal or distal to Rac1 activation. Given the similar time courses of activation for both Rac1 and PI3K, alternative approaches were necessary to elucidate the temporal regulation of these two factors. To this end, we sought to determine whether inhibition of Rac1 by expression of N17Rac1 would impair PI3K activation during rAAV infection. If so, we could conclude that Rac1 functioned upstream of PI3K during AAV-2 endocytosis. HeLa cells were infected with either Ad.N17Rac1 or Ad.CMVLacZ virus 48 h prior to infection with rAAV, and PI3K activity was assessed. As shown in Fig. 5E, N17Rac1 expression inhibited PI3K activation during rAAV infection. These results confirmed our initial hypothesis that Rac1 activation is required for PI3K activation, and hence Rac1 lies proximal to PI3K in the AAV endocytic pathway. Additional evidence evaluating the trypsin sensitivity of virus following wortmannin treatment (discussed below) also supports this hypothesis and suggests that inhibition of PI3K blocks nuclear trafficking but not endocytosis of rAAV.

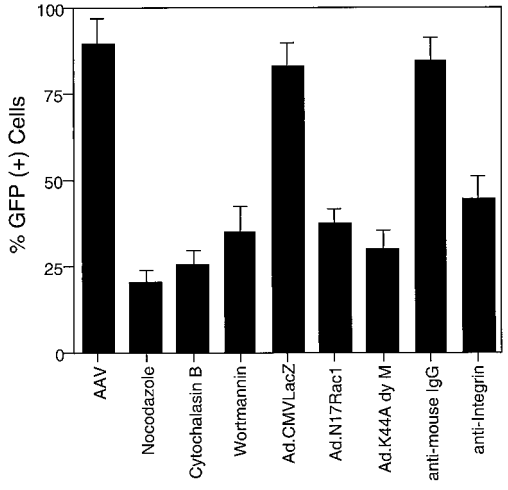

FIG. 8. Inhibitors of AAV-2 endocytosis and nuclear trafficking also reduce rAAV-mediated gene expression. HeLa cells were treated with various agents (indicated below the graph) which modulate AAV-2 endocytosis or nuclear trafficking, and the extent of AV.GFP3ori-mediated GFP expression was analyzed at 35 h postinfection by FACS analysis. For conditions involving infection with recombinant adenoviruses Ad.N17Rac1, Ad.K44Adynamin, and Ad.CMV-LacZ, cells were infected at MOIs of 1,000 particles/cell 48 h prior to AV.GFP3ori infection. Treatments with nocodazole, cytochalasin B, wortmannin, anti-IgG, and anti-integrin were performed as described for Cy3 analyses. All conditions included infection with AV.GFP3ori virus at an MOI of 1,000 DNA particles/cell. FACS analysis data represent the mean ± SEM of four independent data points.

Cytoskeletal involvement in AAV movement to the nucleus. Cytoskeletal changes involving the polymerization of monomeric actin can be induced by the activation of PI3K as well as small GTP-binding proteins such as Rho, Rac, and CDC42 (58). Cytoskeletal elements such as microtubules and microfilaments have long been recognized as important in controlling the intracellular movement of viruses (11, 12, 36). It has also been suggested that microtubules may have a preferential function in the intracellular movement of adenovirus (57), although some reports have also implicated microfilaments in adenovirus infection (46, 49). Therefore, we next sought to characterize the cytoskeletal elements important in the movement of AAV to the nucleus.

Nocodazole treatment to depolymerize microtubules prior to AAV infection resulted in a significant (94.5%) reduction in nuclear accumulation of AAV (Fig. 6A to C). These results are similar to those seen with adenovirus following treatment with nocodazole (57). Cytochalasin B, which disrupts microfilaments, has also been demonstrated to inhibit endocytic processes mediating uptake of adenovirus (46, 49) and papillomavirus (64). Our studies on AAV had similar results, with a dramatic reduction (91%) in nuclear accumulation of AAV following treatment with cytochalasin B (Fig. 6D to F). Thus, these studies indicate that AAV movement to the nucleus is dependent on intact microtubule and microfilament cytoarchitecture. Lastly, disruption of microtubules and microfilaments did not appear to significantly affect the endocytosis of AAV.

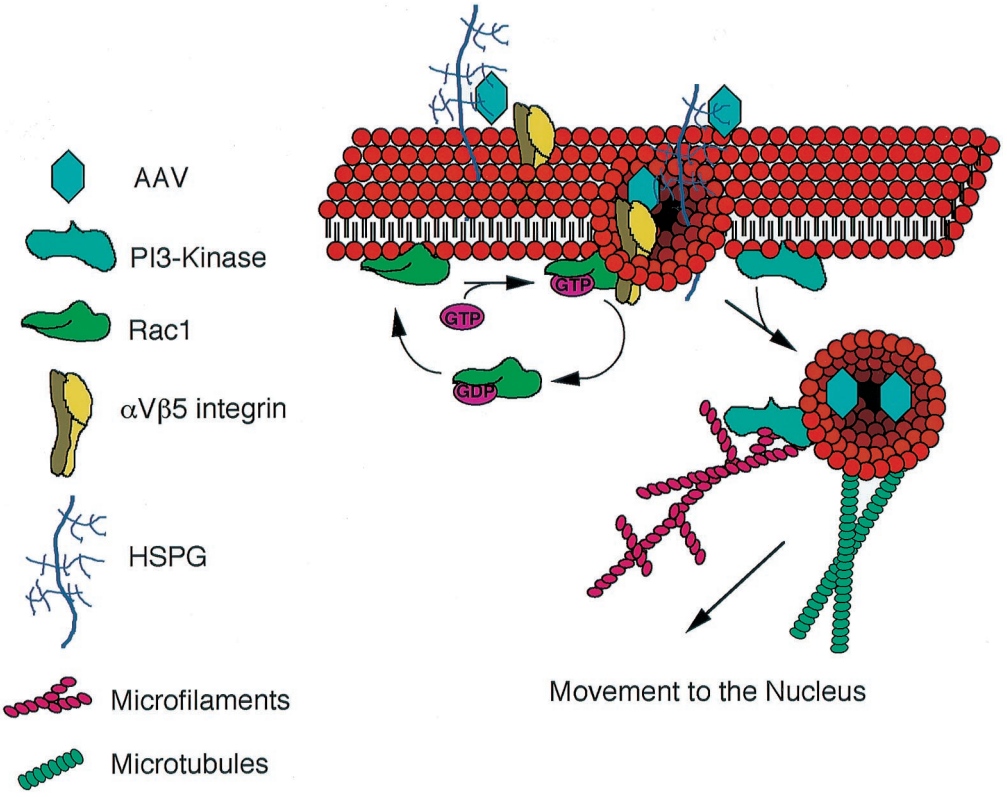

FIG. 9. Schematic representation of AAV-2 endocytic and nuclear trafficking mechanisms. Receptor-mediated endocytosis of AAV-2 in HeLa cells is facilitated through binding to its receptor HSPG and interactions with αVβ5 integrin. Activation of Rac1, potentially by αVβ5 integrin, is required for efficient endocytosis of AAV virus. Following endocytosis, we propose that Rac1 activation leads to stimulation of PI3K pathways, which facilitate the functional rearrangements of the cytoskeleton (microfilaments and microtubules) required for the efficient nuclear targeting of AAV.

Morphologic studies with Cy3-labeled AAV-2 have suggested that PI3K, microtubules, and microfilaments all influence viral transport to the nucleus (Fig. 6G). In contrast, these molecules did not appear to affect AAV-2 endocytosis. However, given the limited resolution of fluorescent microscopy, it was difficult to definitively quantitate membrane-associated AAV-2 as either inside or outside the cell membrane following inhibition of these pathways. Thus, we utilized an alternative approach to evaluate whether wortmannin, nocodazole, or cytochalasin B affected AAV-2 endocytosis. This involved Southern blot analysis to assess the extent of trypsin-resistant viral genomes in nocodazole-, wortmannin-, or cytochalasin B-treated HeLa cells following infection with rAAV. As seen in Fig. 7A, none of these inhibitors affected viral binding for 1 h at 4°C. Similarly, when cells were shifted to 37°C for 2 h, no alterations in the extent of endocytosis were observed, as indicated by trypsin resistance of the internalized viral genomes at this time point (Fig. 7A). These studies conclusively demonstrate that wortmannin, nocodazole, and cytochalasin B do not affect internalization of AAV-2. In contrast, when HeLa cells were infected with rAAV for 2 h and cytoplasmic and nuclear components were fractionated prior to Hirt DNA isolation, all of these inhibitors significantly inhibited nuclear accumulation of viral DNA compared to untreated control cells (Fig. 7B). Together with morphologic observations evaluating nuclear trafficking of AAV-2 in the presence of these inhibitors (Fig. 6G), these molecular studies demonstrate that inhibition of PI3K and microtubule and microfilament polymerization all affect nuclear trafficking of AAV-2 but not endocytosis.

Inhibition of rAAV endocytosis and nuclear trafficking reduce transgene expression from recombinant virus. AV.GFP3ori virus carrying the enhanced green fluorescent protein (EGFP) reporter gene (15) was used to determine whether rAAV-mediated transgene expression was affected by inhibitors of either endocytosis (Ad.N17Rac1, AdK44Adynamin, and αVβ5 integrin blocking antibody) or nuclear trafficking (nocodazole, cytochalasin B, and wortmannin). The dominant mutant dynamin-expressing adenovirus (K44A) was used as a comparative control in these studies and has been previously demonstrated to inhibit endocytosis of rAAV2 and transgene expression in HeLa cells (13). HeLa cells were infected with Ad.N17Rac1, Ad.K44Adynamin, or Ad.CMVLacZ virus 48 h prior to infection with AV.GFP3ori virus at an MOI of 1,000 particles/cell. In addition, HeLa cells were treated with αVβ5 integrin-blocking antibody, nocodazole, cytochalasin B, or wortmannin for 1 h prior to infection with AV.GFP3ori virus. The percentage of cells expressing GFP was determined 35 h postinfection with rAAV by fluorescence-activated cell sorting (FACS) analysis. As seen in Fig. 8, all inhibitors of AAV-2 endocytosis and nuclear trafficking significantly reduced the percentage of GFP-expressing cells compared to untreated and Ad.CMVLacZ-infected cells. The extent of inhibition under each of these conditions was not as complete as observed by morphologic analysis of Cy3AAV or Southern blotting of viral DNA. This may be attributed to the longer time course needed to evaluate transgene expression and the reversibility of the inhibitors used. Furthermore, each of the inhibitors used to block either endocytosis or intracellular transport likely reduces the rate of AAV movement to the nucleus but does not

completely inhibit these processes. Removal of nocodazole 2 h after the infection restored rAAV transduction to 90% of that achieved in the absence of inhibitor, as determined by EGFP expression (data not shown).

DISCUSSION

Mechanisms underlying rAAV transduction have gained considerable interest due to the increasing development of this virus as a vector for gene therapy. Cy3-labeled rAAV has recently become a valuable tool to analyze rAAV transduction (5, 6, 24, 51). In the present study, we have focused on elucidating early steps in the AAV-2 infection process that occur prior to gene conversion of the single-stranded genome to an expressible form in the nucleus. For these analyses, we have utilized Cy3-labeled rAAV virus to enable delineation of the processes controlling AAV-2 entry and intracellular trafficking to the nucleus.

Previous studies have shown that an HSPG receptor mediates binding of AAV-2 to the surface of HeLa cells. The present study has now demonstrated that internalization of HSPG-bound virus occurs through a Rac1-dependent process. Although a direct link between HSPG receptors and Rac1 activation has not been previously identified, integrin and integrin-linked receptors have been shown to play important roles in organizing the actin cytoskeleton through Rac1-dependent intracellular signal transduction pathways (30, 31, 40). Our evidence for the involvement of αVβ5 integrin in rAAV endocytosis further supports this hypothesis. Although no direct evidence exists to date for an interaction between αVβ5 integrin and Rac1, it is reasonable to speculate that AAV-2 interactions with the αVβ5 integrin coreceptor may be responsible for the activation of Rac1 seen during AAV-2 infection. Hence, as shown in Fig. 9, we hypothesize that HSPG receptors on the cell surface may bind AAV-2 and interact with αVβ5 integrin to activate the internalization process, which is facilitated by Rac1-αVβ5 integrin interactions.

Once AAV particles are internalized, triggering steps must occur to start their movement to the nucleus. It is currently unknown whether the virions move to the nucleus within endosomes or whether they break out of endosomes shortly after endocytosis. As previously reported (13) and reproduced in this study (data not shown), persistent colocalization of FITC-labeled transferrin and Cy3AAV within intracellular vesicles near the nucleus suggests that escape of virions from endosomes may occur at or near the nuclear membrane pores. Additionally, confocal localization of Cy3AAV particles inside the nucleus suggests that AAV-2 may be transported through the nuclear pore, a finding which is in stark contrast to studies with adenovirus. Regardless of whether virions reside within endosomes shortly after endocytosis, transport of AAV-2 to the nucleus was greatly inhibited by wortmannin, nocodazole, and cytochalasin B. In contrast, none of these agents appeared to significantly inhibit the binding or endocytosis of AAV-2. These findings suggest that PI3K activation may be necessary to direct virus or virus-containing vesicles along microfilaments and microtubules to the nuclear pores (Fig. 9). Given the link between Rac1 and PI3K pathways in cytoskeleton reorganization, these findings are intriguing.

Several reports have previously suggested that the GTPase Rac1 is a downstream target of PI3K (38, 60). However, in the current study, Rac1 but not PI3K appeared to be necessary for endocytosis. Given the fact that N17Rac1 expression inhibited PI3K activation following rAAV infection, it appears that Rac1 must act proximal to PI3K in the infectious process. Taken together with previous studies in this area, our findings suggest that interactions between Rac1 and PI3K may be bidirectional in nature, depending on the environmental circumstances and stimuli.

In summary, these studies have laid the foundation for a better understanding of AAV-2 infection and the molecular processes that mediate its endocytosis and movement to the nucleus. Given the recent findings that rAAV-2 infection from the apical surface of polarized airway epithelia is significantly impaired by a postendocytic block involving ubiquitination and reduced movement of virus to the nucleus (17), delineation of the intracellular pathways controlling rAAV infection may lead to methods for improving gene delivery with this vector for diseases such as cystic fibrosis.

ACKNOWLEDGMENTS

This work was supported by National Institutes of Health (NHLBI) grant HL58340 (J.F.E.) and the Center for Gene Therapy of Cystic Fibrosis and Other Genetic Diseases (J.F.E.) cofunded by the National Institutes of Health (P30 DK54759) and the Cystic Fibrosis Foundation. We also gratefully acknowledge the University of Iowa DERC (NIDDK) grant DK25295 for tissue culture medium supplies.

We thank Sonya Mehta (University of Iowa image analysis facility) for help during the image analysis. We also extend our gratitude to Tom Moninger and Randy Nessler from the Gene Therapy Center Cell Morphology Core, supported by NIH/NIDDK P30 DK54759, for assistance with confocal microscopy. The Ad.N17Rac1 construct and pGEX-PBD vector encoding GST-PBD were kindly provided by Toren Finkel and Richard Cerione, respectively. We also thank Marty Monick from Garry Hunninghake's laboratory for technical assistance with the PI3K assay. Special thanks go to Terry Ritchie for scientific editing of the paper, Yulong Zhang and Weihong Zhou for assistance with generating the N17Rac1 virus, and Boyd Knosp and Steve Beck from the Image Analysis Facility for 3-D reconstructions and morphometric quantification.

REFERENCES

1. **Alexander, I. E., D. W. Russell, and A. D. Miller.** 1994. DNA-damaging agents greatly increase the transduction of nondividing cells by adeno-associated virus vectors. J. Virol. **68:**8282–8287.
2. **Ali, R. R., M. B. Reichel, A. J. Thrasher, R. J. Levinsky, C. Kinnon, N. Kanuga, D. M. Hunt, and S. S. Bhattacharya.** 1996. Gene transfer into the mouse retina mediated by an adeno-associated viral vector. Hum. Mol. Genet. **5:**591–594.
3. **Andrews, N. C., and D. V. Faller.** 1991. A rapid micropreparation technique for extraction of DNA-binding proteins from limiting numbers of mammalian cells. Nucleic Acids Res. **19:**2499.
4. **Bagrodia, S., S. J. Taylor, K. A. Jordon, L. Van Aelst, and R. A. Cerione.** 1998. A novel regulator of p21-activated kinases. J. Biol. Chem. **273:**23633–23636.
5. **Bartlett, J. S., R. J. Samulski, and T. J. McCown.** 1998. Selective and rapid uptake of adeno-associated virus type 2 in brain. Hum. Gene Ther. **9:**1181–1186.
6. **Bartlett, J. S., R. Wilcher, and R. J. Samulski.** 2000. Infectious entry pathway of adeno-associated virus and adeno-associated virus vectors. J. Virol. **74:**2777–2785.
7. **Bennett, J., D. Duan, J. F. Engelhardt, and A. M. Maguire.** 1997. Real-time, noninvasive in vivo assessment of adeno-associated virus- mediated retinal transduction. Investig. Ophthalmol. Vis. Sci. **38:**2857–2863.
8. **Bokoch, G. M., C. J. Vlahos, Y. Wang, U. G. Knaus, and A. E. Traynor-Kaplan.** 1996. Rac GTPase interacts specifically with phosphatidylinositol 3-kinase. Biochem. J. **315:**775–779.
9. **Brooks, P. C., R. L. Klemke, S. Schon, J. M. Lewis, M. A. Schwartz, and D. A. Cheresh.** 1997. Insulin-like growth factor receptor cooperates with integrin alpha v beta 5 to promote tumor cell dissemination in vivo. J. Clin. Investig. **99:**1390–1398.
10. **Ceresa, B. P., A. W. Kao, S. R. Santeler, and J. E. Pessin.** 1998. Inhibition of clathrin-mediated endocytosis selectively attenuates specific insulin receptor signal transduction pathways. Mol. Cell. Biol. **18:**3862–3870.
11. **Cudmore, S., I. Reckmann, and M. Way.** 1997. Viral manipulations of the actin cytoskeleton. Trends Microbiol. **5:**142–148.
12. **Dramsi, S., and P. Cossart.** 1998. Intracellular pathogens and the actin cytoskeleton. Annu. Rev. Cell Dev. Biol. **14:**137–166.
13. **Duan, D., Q. Li, A. W. Kao, Y. Yue, J. E. Pessin, and J. F. Engelhardt.** 1999. Dynamin is required for recombinant adeno-associated virus type 2 infection. J. Virol. **73:**10371–10376.

14. **Duan, D., P. Sharma, L. Dudus, Y. Zhang, S. Sanlioglu, Z. Yan, Y. Yue, Y. Ye, R. Lester, J. Yang, K. J. Fisher, and J. F. Engelhardt.** 1999. Formation of adeno-associated virus circular genomes is differentially regulated by adenovirus E4 ORF6 and E2a gene expression. J. Virol. **73:**161–169.
15. **Duan, D., P. Sharma, J. Yang, Y. Yue, L. Dudus, Y. Zhang, K. J. Fisher, and J. F. Engelhardt.** 1998. Circular intermediates of recombinant adeno-associated virus have defined structural characteristics responsible for long-term episomal persistence in muscle. J. Virol. **72:**8568–8577.
16. **Duan, D., Y. Yue, and J. F. Engelhardt.** 1999. Response to "polarity influences the efficiency of recombinant adeno-associated virus infection in differentiated airway epithelia." Hum. Gene Ther. **10:**1553–1557.
17. **Duan, D., Y. Yue, Z. Yan, J. Yang, and J. F. Engelhardt.** 2000. Endosomal processing is a major rate limiting step in adeno-associated virus mediated gene transfer to polarized airway epithelia. J. Clin. Investig. **105:**1573–1587.
18. **Engelhardt, J. F., Y. Yang, L. D. Stratford-Perricaudet, E. D. Allen, K. Kozarsky, M. Perricaudet, J. R. Yankaskas, and J. M. Wilson.** 1993. Direct gene transfer of human CFTR into human bronchial epithelia of xenografts with E1-deleted adenoviruses. Nat. Genet. **4:**27–34.
19. **Fasbender, A., J. H. Lee, R. W. Walters, T. O. Moninger, J. Zabner, and M. J. Welsh.** 1998. Incorporation of adenovirus in calcium phosphate precipitates enhances gene transfer to airway epithelia in vitro and in vivo. J. Clin. Investig. **102:**184–193.
20. **Fisher, K. J., G. P. Gao, M. D. Weitzman, R. DeMatteo, J. F. Burda, and J. M. Wilson.** 1996. Transduction with recombinant adeno-associated virus for gene therapy is limited by leading-strand synthesis. J. Virol. **70:**520–532.
21. **Fisher, K. J., K. Jooss, J. Alston, Y. Yang, S. E. Haecker, K. High, R. Pathak, S. E. Raper, and J. M. Wilson.** 1997. Recombinant adeno-associated virus for muscle directed gene therapy. Nat. Med. **3:**306–312.
22. **Flotte, T. R., S. A. Afione, R. Solow, M. L. Drumm, D. Markakis, W. B. Guggino, P. L. Zeitlin, and B. J. Carter.** 1993. Expression of the cystic fibrosis transmembrane conductance regulator from a novel adeno-associated virus promoter. J. Biol. Chem. **268:**3781–3790.
23. **Glaven, J. A., I. Whitehead, S. Bagrodia, R. Kay, and R. A. Cerione.** 1999. The Dbl-related protein, Lfc, localizes to microtubules and mediates the activation of Rac signaling pathways in cells. J. Biol. Chem. **274:**2279–2285.
24. **Hansen, J., K. Qing, H. J. Kwon, C. Mah, and A. Srivastava.** 2000. Impaired intracellular trafficking of adeno-associated virus type 2 vectors limits efficient transduction of murine fibroblasts. J. Virol. **74:**992–996.
25. **Hirt, B.** 1967. Selective extraction of polyoma DNA from infected mouse cell cultures. J. Mol. Biol. **26:**365–369.
26. **Joneson, T., and D. Bar-Sagi.** 1998. A Rac1 effector site controlling mitogenesis through superoxide production. J. Biol. Chem. **273:**17991–17994.
27. **Kao, A. W., B. P. Ceresa, S. R. Santeler, and J. E. Pessin.** 1998. Expression of a dominant interfering dynamin mutant in 3T3L1 adipocytes inhibits GLUT4 endocytosis without affecting insulin signaling. J. Biol. Chem. **273:**25450–25457.
28. **Kapeller, R., and L. C. Cantley.** 1994. Phosphatidylinositol 3-kinase. Bioessays **16:**565–576.
29. **Kaplitt, M. G., P. Leone, R. J. Samulski, X. Xiao, D. W. Pfaff, K. L. O'Malley, and M. J. During.** 1994. Long-term gene expression and phenotypic correction using adeno-associated virus vectors in the mammalian brain. Nat. Genet. **8:**148–154.
30. **Keely, P. J., J. K. Westwick, I. P. Whitehead, C. J. Der, and L. V. Parise.** 1997. Cdc42 and Rac1 induce integrin-mediated cell motility and invasiveness through PI(3)K. Nature **390:**632–636.
31. **Kheradmand, F., E. Werner, P. Tremble, M. Symons, and Z. Werb.** 1998. Role of Rac1 and oxygen radicals in collagenase-1 expression induced by cell shape change. Science **280:**898–902.
32. **Kim, K. S., K. Takeda, R. Sethi, J. B. Pracyk, K. Tanaka, Y. F. Zhou, Z. X. Yu, V. J. Ferrans, J. T. Bruder, I. Kovesdi, K. Irani, P. Goldschmidt-Clermont, and T. Finkel.** 1998. Protection from reoxygenation injury by inhibition of rac1. J. Clin. Investig. **101:**1821–1826.
33. **Klemke, R. L., S. Cai, A. L. Giannini, P. J. Gallagher, P. de Lanerolle, and D. A. Cheresh.** 1997. Regulation of cell motility by mitogen-activated protein kinase. J. Cell Biol. **137:**481–492.
34. **Leopold, P. L., B. Ferris, I. Grinberg, S. Worgall, N. R. Hackett, and R. G. Crystal.** 1998. Fluorescent virions: dynamic tracking of the pathway of adenoviral gene transfer vectors in living cells. Hum. Gene Ther. **9:**367–378.
35. **Li, E., D. Stupack, G. M. Bokoch, and G. R. Nemerow.** 1998. Adenovirus endocytosis requires actin cytoskeleton reorganization mediated by Rho family GTPases. J. Virol. **72:**8806–8812.
36. **Luftig, R. B., and L. D. Lupo.** 1994. Viral interactions with the host-cell cytoskeleton: the role of retroviral proteases. Trends Microbiol. **2:**178–182.
37. **Memmo, L. M., and P. McKeown-Longo.** 1998. The alphavbeta5 integrin functions as an endocytic receptor for vitronectin. J. Cell Sci. **111:**425–433.
38. **Missy, K., V. Van Poucke, P. Raynal, C. Viala, G. Mauco, M. Plantavid, H. Chap, and B. Payrastre.** 1998. Lipid products of phosphoinositide 3-kinase interact with Rac1 GTPase and stimulate GDP dissociation. J. Biol. Chem. **273:**30279–30286.
39. **Miyamoto, S., S. K. Akiyama, and K. M. Yamada.** 1995. Synergistic roles for receptor occupancy and aggregation in integrin transmembrane function. Science **267:**883–885.
40. **Miyamoto, S., H. Teramoto, O. A. Coso, J. S. Gutkind, P. D. Burbelo, S. K. Akiyama, and K. M. Yamada.** 1995. Integrin function: molecular hierarchies of cytoskeletal and signaling molecules. J. Cell Biol. **131:**791–805.
41. **Ng, T., D. Shima, A. Squire, P. I. Bastiaens, S. Gschmeissner, M. J. Humphries, and P. J. Parker.** 1999. PKCalpha regulates beta1 integrin-dependent cell motility through association and control of integrin traffic. EMBO J. **18:**3909–3923.
42. **Nobes, C. D., and A. Hall.** 1995. Rho, rac, and cdc42 GTPases regulate the assembly of multimolecular focal complexes associated with actin stress fibers, lamellipodia, and filopodia. Cell **81:**53–62.
43. **Odorizzi, G., M. Babst, and S. D. Emr.** 1998. Fab1p PtdIns(3)P 5-kinase function essential for protein sorting in the multivesicular body. Cell **95:**847–858.
44. **Olson, M. F., A. Ashworth, and A. Hall.** 1995. An essential role for Rho, Rac, and Cdc42 GTPases in cell cycle progression through G1. Science **269:**1270–1272.
45. **Parsons, J. T.** 1996. Integrin-mediated signalling: regulation by protein tyrosine kinases and small GTP-binding proteins. Curr. Opin. Cell Biol. **8:**146–152.
46. **Patterson, S., and W. C. Russell.** 1983. Ultrastructural and immunofluorescence studies of early events in adenovirus-HeLa cell interactions. J. Gen. Virol. **64:**1091–1099.
47. **Qing, K., C. Mah, J. Hansen, S. Zhou, V. Dwarki, and A. Srivastava.** 1999. Human fibroblast growth factor receptor 1 is a co-receptor for infection by adeno-associated virus 2. Nat. Med. **5:**71–77.
48. **Qing, K., X. S. Wang, D. M. Kube, S. Ponnazhagan, A. Bajpai, and A. Srivastava.** 1997. Role of tyrosine phosphorylation of a cellular protein in adeno- associated virus 2-mediated transgene expression. Proc. Natl. Acad. Sci. USA **94:**10879–10884.
49. **Qiu, C., M. B. De Young, A. Finn, and D. A. Dichek.** 1998. Cationic liposomes enhance adenovirus entry via a pathway independent of the fiber receptor and alpha(v)-integrins. Hum. Gene Ther. **9:**507–520.
50. **Salvetti, A., S. Oreve, G. Chadeuf, D. Favre, Y. Cherel, P. Champion-Arnaud, J. David-Ameline, and P. Moullier.** 1998. Factors influencing recombinant adeno-associated virus production. Hum. Gene Ther. **9:**695–706.
51. **Sanlioglu, S., P. Benson, and J. F. Engelhardt.** 2000. Loss of ATM function enhances recombinant adeno-associated virus transduction and integration through pathways similar to UV irradiation. Virology **268:**68–78.
52. **Sanlioglu, S., D. Duan, and J. F. Engelhardt.** 1999. Two independent molecular pathways for recombinant Adeno-Associated virus genome conversion occur after UV-C and E4orf6 augmentation of transduction. Hum. Gene Ther. **10:**591–602.
53. **Sanlioglu, S., and J. Engelhardt.** 1999. Cellular redox state alters recombinant adeno-associated virus transduction through tyrosine phosphatase pathways. Gene Ther. **6:**1427–1437.
54. **Seksek, O., J. Biwersi, and A. S. Verkman.** 1997. Translational diffusion of macromolecule-sized solutes in cytoplasm and nucleus. J. Cell Biol. **138:**131–142.
55. **Summerford, C., J. S. Bartlett, and R. J. Samulski.** 1999. AlphaVbeta5 integrin: a co-receptor for adeno-associated virus type 2 infection. Nat. Med. **5:**78–82.
56. **Summerford, C., and R. J. Samulski.** 1998. Membrane-associated heparan sulfate proteoglycan is a receptor for adeno-associated virus type 2 virions. J. Virol. **72:**1438–1445.
57. **Suomalainen, M., M. Y. Nakano, S. Keller, K. Boucke, R. P. Stidwill, and U. F. Greber.** 1999. Microtubule-dependent plus- and minus end-directed motilities are competing processes for nuclear targeting of adenovirus. J. Cell Biol. **144:**657–672.
58. **Tapon, N., and A. Hall.** 1997. Rho, Rac and Cdc42 GTPases regulate the organization of the actin cytoskeleton. Curr. Opin. Cell Biol. **9:**86–92.
59. **Tolias, K. F., L. C. Cantley, and C. L. Carpenter.** 1995. Rho family GTPases bind to phosphoinositide kinases. J. Biol. Chem. **270:**17656–17659.
60. **Valgeirsdottir, S., L. Claesson-Welsh, E. Bongcam-Rudloff, U. Hellman, B. Westermark, and C. H. Heldin.** 1998. PDGF induces reorganization of vimentin filaments. J. Cell Sci. **111:**1973–1980.
61. **Wang, K., S. Huang, A. Kapoor-Munshi, and G. Nemerow.** 1998. Adenovirus internalization and infection require dynamin. J. Virol. **72:**3455–3458.
62. **Wayner, E. A., R. A. Orlando, and D. A. Cheresh.** 1991. Integrins alpha v beta 3 and alpha v beta 5 contribute to cell attachment to vitronectin but differentially distribute on the cell surface. J. Cell Biol. **113:**919–929.
63. **Xiao, X., J. Li, and R. J. Samulski.** 1996. Efficient long-term gene transfer into muscle tissue of immunocompetent mice by adeno-associated virus vector. J. Virol. **70:**8098–8108.
64. **Zhou, J., L. Gissmann, H. Zentgraf, H. Muller, M. Picken, and M. Muller.** 1995. Early phase in the infection of cultured cells with papillomavirus virions. Virology **214:**167–176.